EDSU Journal of Engineering and Technology (EDSUJET) Vol. 2 (1), pp. 120 – 136. 2026
ISSN (Print):3121 – 8725 eISSN (Online): 3121 – 8597

EDSU Journal of Engineering and Technology (EDSUJET)

Development and Optimization of a High Efficiency Sawdust Briquette Machine for Sustainable Energy Production

Chinyere Joy Emenyeonu[1)]* and Vincent Aizebeoje Balogun[2)]

[1), 2)] *Department of Mechanical Engineering, Edo State University, Uzairue, Edo State, Nigeria*
***Coresponding author email address**[*]: dennisjoy133@gmail.com;*

Received: 1st November 2025, Accepted: 21st January 2026, Published: 31 March 2026

K E Y W O R D S

Briquetting
Sawdust
Biomass
Optimization
Calorific
Sustainability

A B S T R A C T

The efficiency of agricultural waste briquettes for domestic and industrial applications hinges on their fuel properties. This research focused on briquettes created from mahogany and iroko hardwood residues. These residues were sun-dried and sieved into various particles size before being composition of the briquettes. The findings indicate that both types sever as viable biomass fuels, with mahogany briquettes exhibiting superior attributes compared to iroko. Optimal results were identified at a particle diameter of 0.85 mm using mahogany. Yielding a briquette with a density of 0.8390 kg/m. compaction pressure of 1.4669 N/m, moisture content of 31.39%, and a calorific value of 28.953 Kj/kg. The optimization process highlighted a desirability function of 0.4393, underscoring the effectiveness of the selected parameters.

INTRODUCTION

The rising global energy demand and the depletion of fossil fuel reserves have intensified the search for sustainable and renewable energy alternatives. Biomass, particularly sawdust, has gained significant attention due to its abundance, renewability, and carbon-neutral nature (Mao et al., 2020; Kumar & Sadh, 2021; Owusu, 2025; Roman & Grzegorzewska, 2024). Sawdust is a major byproduct of wood-processing industries and is often improperly disposed of, creating environmental challenges (Veeravalli et al., 2024; Onyegirim et al., 2025). However, when densified into briquettes, sawdust becomes a valuable solid fuel suitable for domestic and industrial energy applications, thereby addressing both waste management and energy needs (Mao et al., 2020; Khalid et al., 2025).
Studies have demonstrated the environmental and energy benefits of sawdust briquettes. Khalid et al. (2025) reported lower carbon monoxide emissions from sawdust briquettes compared to coal, while Owusu (2025) showed that optimized feedstock blending improves calorific value and mechanical strength. Similarly, Roman and Grzegorzewska (2024) and Akowuah et al. (2012) confirmed that forest biomass residues and sawdust charcoal briquettes exhibit favorable fuel properties and reduced greenhouse gas emissions.

Briquetting is an efficient and cost-effective densification process that improves the handling, storage, and combustion characteristics of biomass (Kumar & Sadh, 2021; Haldorai et al.,

2022). Advances in briquetting machine design such as hydraulic, screw, and piston presses have focused on optimizing pressure, temperature, and moisture content to enhance briquette quality and production efficiency (Pandey et al., 2020; Veeravalli et al., 2024). Improved machine configurations have been shown to significantly increase output and fuel performance (Onyegirim et al., 2025).

The properties of briquettes, including green density, moisture content, and burning rate, are critical indicators of fuel quality. Higher green density generally results in greater energy content and longer burning time, while excessive moisture negatively affects ignition and combustion efficiency (Akinbomi et al., 2025; Kumar & Sadh, 2021). An optimal burning rate ensures efficient and controlled energy release during use (Haldorai et al., 2022).
This study focuses on the design, development, and optimization of a high-efficiency sawdust briquette machine aimed at improving biomass energy production. Emphasis is placed on machine parameters, binder selection, and feedstock composition to produce high-quality briquettes that support sustainable energy development and environmental protection (Mao et al., 2020; Geberehiwot et al., 2025).

2. MATERIALS AND METHODS

The study involved designing a manually operated briquetting machine and evaluating the production and properties of mahogany and iroko briquettes. Key analyses included density, compaction pressure, ash content, crushing strength, boiling rate, and calorific value, with sieve analysis and RSM optimization applied to assess performance.

Figure 1 A briquetting Making Machine

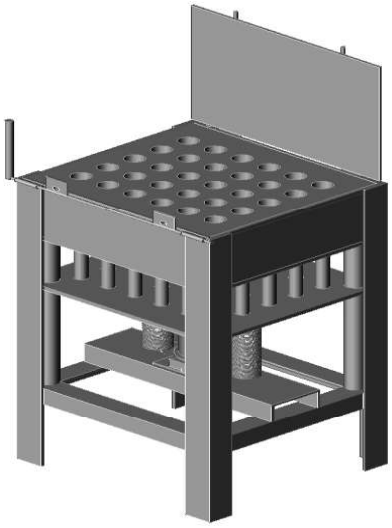

Figure 2: AutoCad Drawing of Briquetting Machine

Table 1: Briquetting Machine Components

S/N	PART
1.	Cover Plate
2.	Cylindrical Hole for Brigquettes
3.	Encasement for Cylinder
4.	Bolt & Nut Assembly
5.	Pressing Plate Assembly
6.	Piston Rod
7.	Hydraulic Jack
8.	Spring
9.	Base Support
10.	Frame Support
NAME	EMENYEONU CHINYERE JOY
DRAWN BY	EMENYEONU CHINYERE JOY
DIMENSION	MM
DATE	20TH MARCH, 2025

2.1 Design Consideration

The machine was designed to apply a compaction pressure of 0.2–10 MPa for effective briquette formation with minimal manual effort. A helical spring aids controlled compression, while 30 struts and compaction cylinders enable the production of 30 briquettes per cycle.

2.1.1 Description of Parts and Functions

The briquetting machine consists of a frame support for stability, a hydraulic jack for compression, and a return spring for reset. It also includes a bottom plate, strut, compaction cylinder, top plate, and upper compaction plate to ensure uniform force during briquette

formation.

2.1.2 The Main Frame and Mould

The main frame measures 750 mm × 318 mm × 159 mm and is welded into a rectangular structure. The upper section, above the mould, is made of 6 mm thick mild steel plate formed into a box shape.

2.1.3 Function

The mould has the following functions:

i. The chamber where the compression of the material occur.
ii. It gives the press its essence
iii. It affords the briquettes its basic cylindrical shape

2.1.4 The Bottom Plate

The bottom plate is made of 6 mm thick mild steel plate and has a length of 312 mm, considering the plate as thin cylindrical shell, the tensile stress acting in a direction tangential to the circumference is given by

$$\sigma c = \frac{pd}{2t} \quad (1)$$

Where σ_c= Circumferential stress in N/m^2
d = internal diameter of the shell.
t = thickness of the shell (plate)
p = intensity of t the internal pressure.
For mild steel material, the circumferential stress is numerically equal to 0.8 times the yield point stress of the material (Khurmi and Gupta, 1980). Taken the Yield strength of mild steel in tension as 250 Mpa,
σ_c= 0.8 x 250 =200 MPa
Substituting the values into equation3.1 and also considering the Compacting pressure of 10 MPa
t = 3.975 mm
Where d is numerically equal to the height of the load = 159 mm
Using a factor of safety of 1.5
t =15 x 3.975 = 5.962 mm $\cong$6 mm
To determine the speed,

$$V=\frac{d}{t} \quad (2)$$

$$= V=\frac{0.159}{120}=0.001325 \text{ m/s}$$

2.1.5 The Cover Plate

The cover plate covers the mould and it act as a piston which compresses the material.

2.1.6 Design Procedure for Compression of Helical Spring

Spring material = Carbon Steel

The permissible stress for carbon steel for average service obtained from standard tables =385 Mpa and the corresponding modulus of rigidity, G=8 GN/m^2 (Sharma and Aggarwal 1999).
For stability, size and efficient use of the material, a spring index of 6 is selected.
But spring index,

$$S = \frac{d}{d} \quad (3)$$

Where D = mean coil diameter
D = wire diameter
To accommodate the effect of curvature and direct shear, the Wahl's correction factor, C is obtained as:

$$C = \frac{4s-1}{4s-4} + \frac{0.615}{s} \quad (4)$$

$$C = \frac{4\ x\ 6-1}{4x6-4} + \frac{0.615}{6} = 1.2525$$

For a start, a mean coil diameter of D =37.5 mm is assumed.
The wire diameter, d is therefore obtained from the relation.

$$\sigma = \frac{8\ w\ d}{nd3}\ c \quad (5)$$

Where σ = permissible shear stress
W= maximum load for the spring material
W= crushing strength x total area of briquette

The crushing strength of 0.1137 m diameter of mahogany briquette was obtained experimentally as 4340.63 x 0.11368= 493.44 N
Substituting the values into equation (6)
D=0.00535 mm =5.35 mm
From standard table, a standard wire size of d=5.893 with SWG/4 is selected .
Thus, the actual value of S is given by

$$S = \frac{8\ W\ D3\ n}{Gd4} \quad (7)$$

Where $\delta = deflection\ of\ spring.$
Since this is a compression spring, the deflection will be small.
Assuming a reflection of 12.5 mm, the number of turns.

$$n = \frac{\delta\ \times\ G \times d4}{8 \times\ W\ \times D \times\ 3}$$

$$n\ = \frac{0.0125\ \times\ 80\ x\ 10(9) \times (0.005893)4}{8\ \times 493.44\ \times\ (0.03748)3}$$

$$n\ = \frac{1.205996}{0.20951} = 5.76 = 6$$

using factor of safety as 2.5 for fatigue loading.
n = 6 x 2.5 =15 (n x N)
Since this a compression spring, a total of 1.82 in inactive turns is allowed so that the effective number of turns.
n^1 = n + 1.82
n^1 = 15+ 1.82=16.82 =17 turns
the spring rate, K is given by

K = $\frac{W}{\delta}$= $\frac{493.44}{12.5}$ =39.48 N/mm

The solid length, Ls= n^1d=17 x 5.893 = 100.181 mm

The free length, LF = n^1d + $\boldsymbol{\delta max}$ =0.15 m$\boldsymbol{\delta max}$

Lf = 100.181 + 12.5 +0.15 x 12.5 +114.556 mm

Use Lf=120 mm for safe clearance

The pitch of the spring.

$$P = \frac{\text{free length}}{n^1 - 1} = \frac{120}{17 - 1} = \frac{120}{6} = 7.5\ mm$$

Provision for burkling effect

Using

W_{er}= K x K_B x Lf

Where

W_{cr} = critical axial load

K = spring rate

K_B = bulking factor depending upon the ratio Lf/D

For $\frac{Lf}{D} = \frac{120}{37.48}$

K_B = 0.71 for built –in end spring (obtained from standard tables)

Wcr = 39.48 x0.71 x 120 = 3363.69N

Since W<Wcr, the spring is safe

Therefore, the design parameters are:

Wire diameter, d =5.893 mm

Number of turns = 17

Free length, Lf=m 120 mm

Solid length Ls=100.181 mm

Pitch, P= 7.5 m

With the designed parameters, the spring was carefully selected.

2.2 Density analysis of mahogany briquettes and iroko briquettes

The formula below was used to determine their various densities

$$\text{Density } (\rho) = \frac{mass\ (m)}{volume\ (V)} \quad (8)$$

The volume of briquettes made from mahogany and IROKO briquettes were determined by this formula

$$V = \frac{\pi d2h}{4} \quad (9)$$

The calculations can be found in Appendix 2 section 2.1.1

For the Area, this formula was used:

$$A = \pi d\{h + \frac{d}{2}\} \quad (10)$$

2.3 Compaction pressure analysis of mahogany and iroko briquette

The formula below was used to determine the compaction pressure of the briquettes.

$$\text{Pressure} = \frac{Force}{Area} \quad (11)$$

Where force = Ma

The calculations can be found in Appendix 2 sections 2.3.0 and 2.3.1

2.4 Sieve Analysis

Mahogany and iroko hardwood wastes were sun-dried, ground, and sieved to particle sizes of 0.6–6.35 mm. Samples were oven-dried at 110 °C for 2.5 hours, cooled, and crushed for uniformity. The manually operated briquetting machine applies 0.2–10 MPa compaction using a helical spring and produces 30 briquettes per cycle via multiple struts and compaction cylinders.

2.5 Ash Content analysis of mahogany briquettes and iroko briquette

The muffle furnace was used to determine the ash content of mahogany and iroko briquettes, calculated using Equation 1.

$$\text{Percentage Ash content} = \frac{Loss\ in\ weight}{Weight\ of\ sample+crucible} \times \frac{100}{1} \quad (12)$$

Boiling rate of mahogany and iroko briquette

Five briquettes of varying particle sizes were tested on a charcoal stove to determine boiling rate. An aluminum pot containing 1600 ml of water was used, and a digital thermocouple recorded temperature and time to boil for each sample. The briquette cross-sectional area was used with Equation 2 to determine crushing strength.

$$Crushing\ Strength = \frac{Maximum\ load}{Total\ Area\ of\ Briquettes} \quad (13)$$

Calorific value analysis of mahogany briquettes and iroko briquette

The heat values of the briquettes were measured using a bomb calorimeter, and 12 experimental runs were conducted with RSM in Design-Expert (v6.0.6), varying briquette diameter at six levels and biomass type at two levels.

Table 1: Experimental Design BY Design Expert Software Version 6.0.6

Std	Run	Block	Factor 1A: Diameter Mm	Factor 2B: Biomass Type
2	1	Block 1	0.60	Mahogany
5	2	Block 1	1.40	Mahogany
10	3	Block 1	2.00	Mahogany
11	4	Block 1	2.40	Mahogany
4	5	Block 1	3.35	Mahogany
3	6	Block 1	6.35	Mahogany
6	7	Block 1	0.60	Iroko
1	8	Block 1	1.40	Iroko
12	9	Block 1	2.00	Iroko
9	10	Block 1	2.40	Iroko
7	11	Block 1	3.35	Iroko
8	12	Block 1	6.35	Iroko

Table 1 shows that 12 runs were made, the input factors were the diameter of the briquette and biomass type. The diameters of the briquette were varied at 6 levels while the biomass types were varied at 2 levels. The responses were inputted for each run accordingly and analyzed using analysis of variance (ANOVA) and regression analysis interface of the software. Quadratic model was used all through for all the responses (Y), and it is a second order

polynomial regression in the order of

$$Y = \beta_0 + \beta_1 X_1, + \beta_2 X_2 + \beta_{12} X_1, X_2, + \beta_{11} X_1^2 + \beta_{22} X_2^2 + \in. \quad (14)$$

3.0 RESULTS AND DISCUSSION

3.1 Density analysis of mahogany briquettes

Table 2: Density Analysis of mahogany Briquettes Values

Diameter(mm)	Mass(g)	Volume($m^{3)}$
0.60	22.40	0.0170
1.40	20.50	0.0924
2.00	16.10	0.1885
2.40	14.20	0.2715
3.35	12.20	0.5289
6.35	12.00	1.9004

Table 2 indicates that as particle size increased from 0.60 mm to 6.35 mm, briquette mass decreased from 22.40 g to 12.00 g, while volume increased from 0.0170 m^3 to 1.9004 m^3, resulting in lower density. This confirms that finer particles produce denser briquettes than coarser particles.

3.1.2 Density analysis of Iroko briquettes

The densities of iroko briquettes were calculated from their mass and volume, showing that lower mass corresponds to higher volume, indicating increased briquette expansion.

Table 3: Density analysis of Iroko briquettes values

Diameter(mm)	Mass(g)	Volume($m^{3)}$
0.60	22.60	0.0170
1.40	20.60	0.0924
2.00	20.00	0.1885
2.40	19.60	0.2715
3.35	18.70	0.5289
6.35	16.70	1.9004

Table 3 shows the density analysis of iroko briquettes across different particle sizes. As particle size increases from 0.60 mm to 6.35 mm, the mass decreases from 22.60 g to 16.70 g, while the volume increases from 0.0170 m^3 to 1.9004 m^3. This indicates that finer particles produce denser, more compact briquettes, whereas coarser particles result in larger, less dense briquettes, which can influence combustion efficiency and handling characteristics.

3.2 Compaction pressure analysis of mahogany briquettes

Table 4 shows that as particle size increases from 0.60 mm to 6.35 mm, briquette mass decreases from 22.40 g to 12.00 g while area increases from 0.11368 m^2 to 1.26045 m^2. This indicates finer particles yield denser, more compact briquettes, whereas coarser particles produce larger, less dense briquettes.

3.3 Compaction pressure analysis of iroko briquettes

The values on Tables 4 were used to determine the compaction pressure of various sizes of iroko briquettes. The diameter, area and masses were considered and this resulted to the compaction pressure being determined.

Table 4: Compaction pressure analysis of mahogany briquettes values

Diameter (mm)	Area (m²)	Mass (g)
0.60	0.11368	22.40
1.40	0.28701	20.50
2.00	0.38332	16.10
2.40	0.46150	14.20
3.35	0.69173	12.20
6.35	1.26045	12.00

Table 5: Compaction Pressure Analysis of Iroko Briquettes

Diameter (mm)	Area (m²)	Mass (g)
0.60	0.11368	23.60
1.40	0.28701	20.60
2.00	0.38332	20.00
2.40	0.46150	19.60
3.35	0.69173	18.70
6.35	1.26045	16.70

The compaction pressure of mahogany and iroko briquettes was determined using standard pressure calculations. Results show that the briquette area increased from 0.11368 m² at 0.60 mm particle size to 1.26045 m² at 6.35 mm. This indicates that briquettes with higher mass require greater compaction pressure, as increased mass demands higher force during compaction.

3.4 Moisture Content analysis of mahogany briquettes

The values on Table 5 were used to determine the moisture content of various sizes of mahogany briquettes, the values were obtained from the experimental analysis that was done when considering the diameter, weight of a sample before and after heating.

Table 6: Weight of Samples Before and After Heating

Diameter (mm)	Weight Before Heating (g)	Weight After Heating (g)
0.60	23.60	17.70
1.40	20.60	15.26
2.00	20.00	14.80
2.40	19.60	12.30
3.35	18.70	11.35
6.35	16.70	9.85

Table 6 shows a consistent reduction in sample weight after heating across all briquette diameters. The weight before heating decreased from 23.60 g at 0.60 mm to 16.70 g at 6.35 mm, while the corresponding weight after heating reduced from 17.70 g to 9.85 g. This weight loss indicates moisture and volatile matter removal during heating, with larger diameters exhibiting greater absolute weight reduction.

3.5 Moisture content analysis of Iroko briquettes

Table 7: Moisture content analysis of Iroko briquettes values

Diameter(mm)	Weight of sample before heating(g)	Weight of sample after heating(g)
0.60	22.4	14.70
1.40	20.5	13.60
2.00	16.1	12.10
2.40	14.2	10.90
3.35	12.2	10.10
6.35	12.0	10.00

Table 7 shows that finer briquettes (0.60 mm) retained the most mass after heating (17.70 g from 23.60 g; 14.7 kg from 22.4 kg), while coarser briquettes (6.35 mm) retained the least (9.85 g from 16.70 g; 10.0 kg from 12.0 kg), indicating higher moisture content in finer particles.

3.6 Calorific value analysis of Iroko briquettes

The values on Table 8 were used to determine the calorific value of iroko Briquettes. The result shows that the briquette made from iroko having 0.60 mm diameter has the highest calorific value of 30.380 mj/kg while 6.35 mm diameter has the lowest calorific value of 13.056 mj/kg, it implies that the finer the particle sizes of the briquettes the higher the calorific value.

Table 8: Calorific value analysis of iroko briquettes

Diameter (mm)	Calorific value mj/hg
0.60	30.380
1.40	28.308
2.00	18.354
2.40	16.354
3.35	14.008
6.35	13.056

Sieve analysis report (dry sieve process) working sheet (M1=300g)

Table 8 shows the value obtain from dry sieve analysis shows the various test sieve used, the quality of mass retained, the percentage of sample retained and also the cumulative percentage passing. From the result, it was discovered that the sieve having the highest diameter of 6.35 mm retain the least amount of sample of 3.1g and a cumulative percentage passing of 35.61%. This implies that the higher the diameter of the sieve the higher the cumulative percentage is passing. There is also a variation in the masses retained due to its sieving processes and nature of the sample.

The Iroko sample in Table 9 is mainly medium-grained, with the highest retention on the 1.40 mm sieve (26.22%). Coarse particles are minimal, and fines are very low, with no material passing the 0.063 mm sieve. Overall, the material is well graded and clean, suitable for efficient processing and performance

Table 9: Iroko sieve analysis result

S/N	BS Test Sieve Mm	Mass retained (g)	Percentage Retained (m.m1)×100	Cumulative Percentage Passing
1	6.35	3.1	1.04	98.97
2	3.35	53.4	17.90	81.07
3	2.36	38.9	13.04	68.03
4	2.00	18.5	6.20	61.83
5	1.40	78.2	26.22	35.61
6	1.18	22.6	7.58	28.03
7	0.600	45.6	15.29	12.74
8	0.425	14.6	4.90	7.84
9	0.300	7.4	2.48	5.36
10	0.212	5.8	1.95	3.42
11	0.150	3.2	1.07	2.35
12	0.063	7.0	2.35	0
	TOTAL MASS RETAINED	**298.3**		

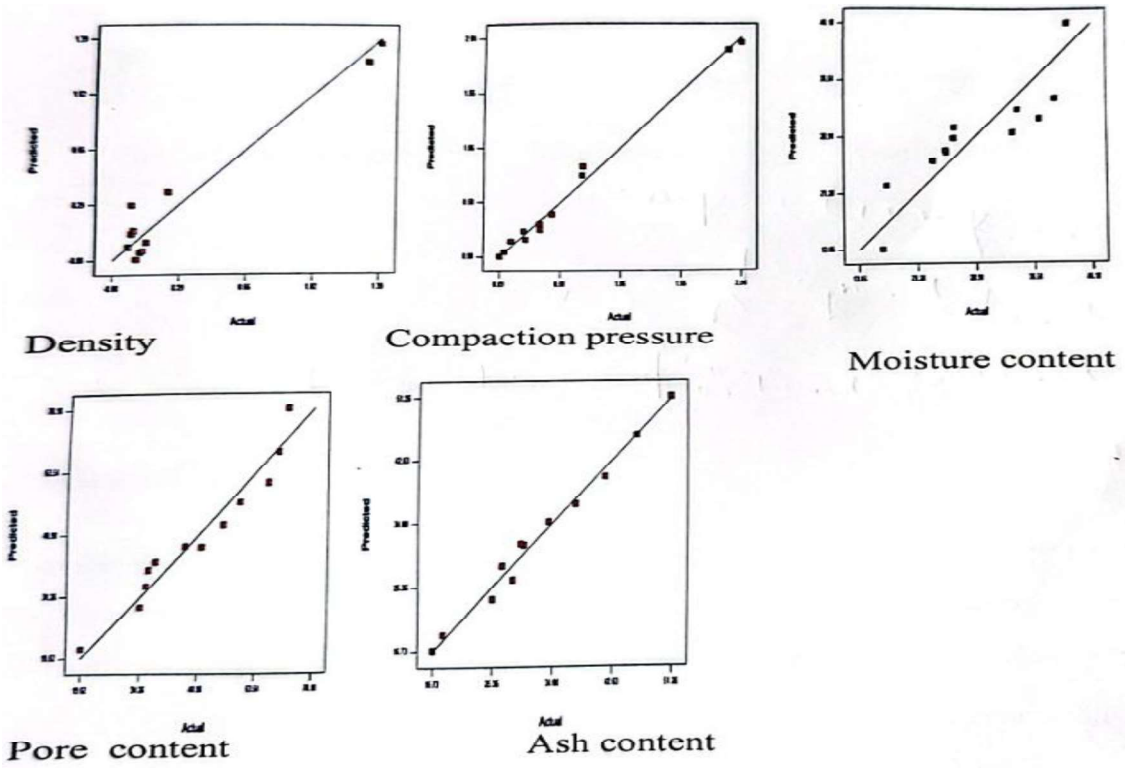

Figure 3: *Model validation presentation*

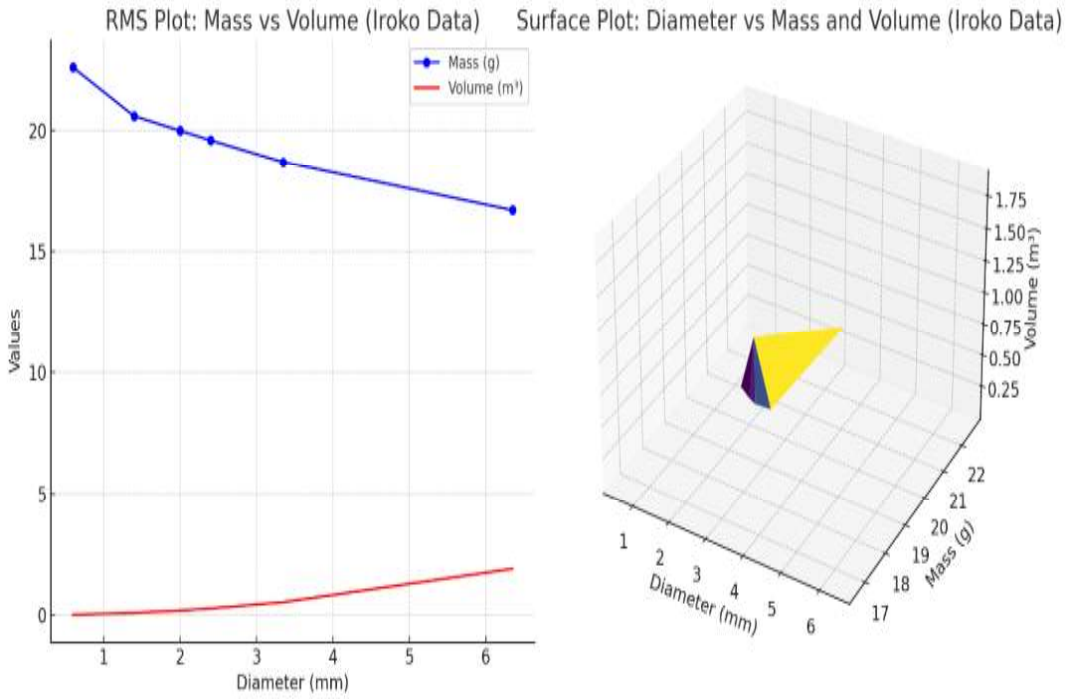

Figure 4: ***(a)*** *RMS plot: Mass versus Volume Surface plot* ***(b)*** *Diameter versus mass and volume*

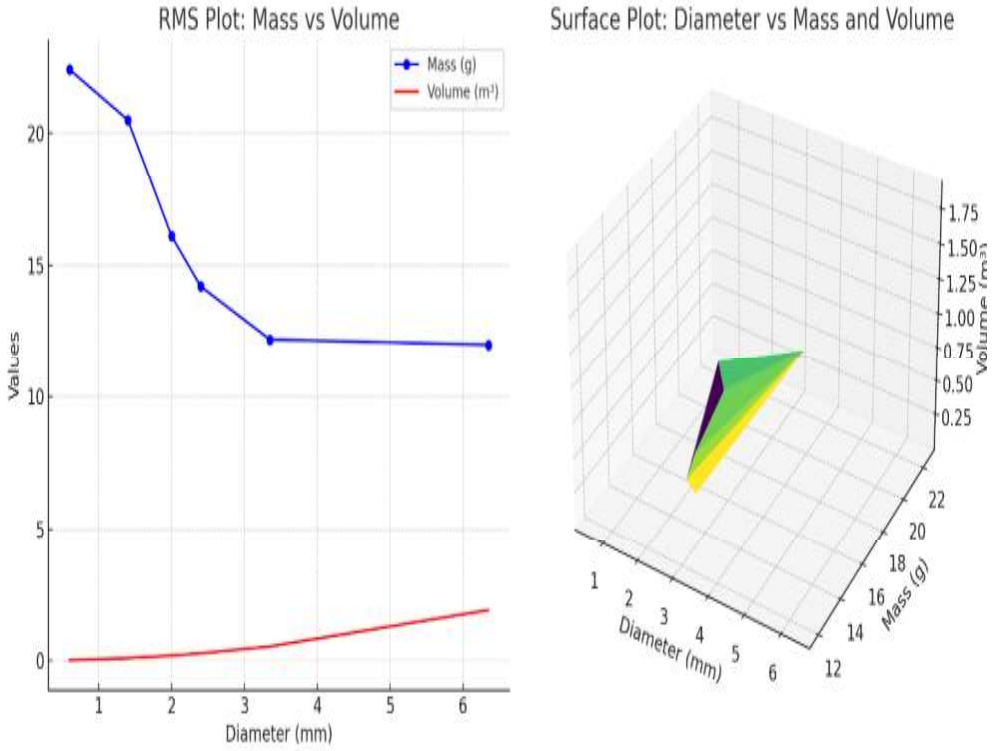

Figure 5: ***(a)*** *RMS plot: Mass Versus Volume (Iroko data)* ***(b)*** *Surface plot: Diameter versus mass and volume (Iroko date)*

The figure 3 consists of two distinct visual representations that together describe the relationship among diameter, mass, and volume of the measured samples of Mahogany Briquettes. On the left side is the RMS Plot labeled "Mass vs Volume," while on the right side is the Surface Plot labeled "Diameter vs Mass and Volume."

The RMS plot in Figure 4 presents diameter (mm) on the x-axis and mass (g) and volume (m^3) on the y-axis. Mass (blue curve) drops sharply between 1–3 mm and then levels off up to 6 mm, indicating higher density at smaller diameters. Conversely, volume (red curve) increases steadily and nonlinearly with diameter, consistent with the cubic relationship between size and volume. Overall, the figure highlights the complementary behavior of mass reduction and volume growth with increasing diameter for Iroko wood samples.

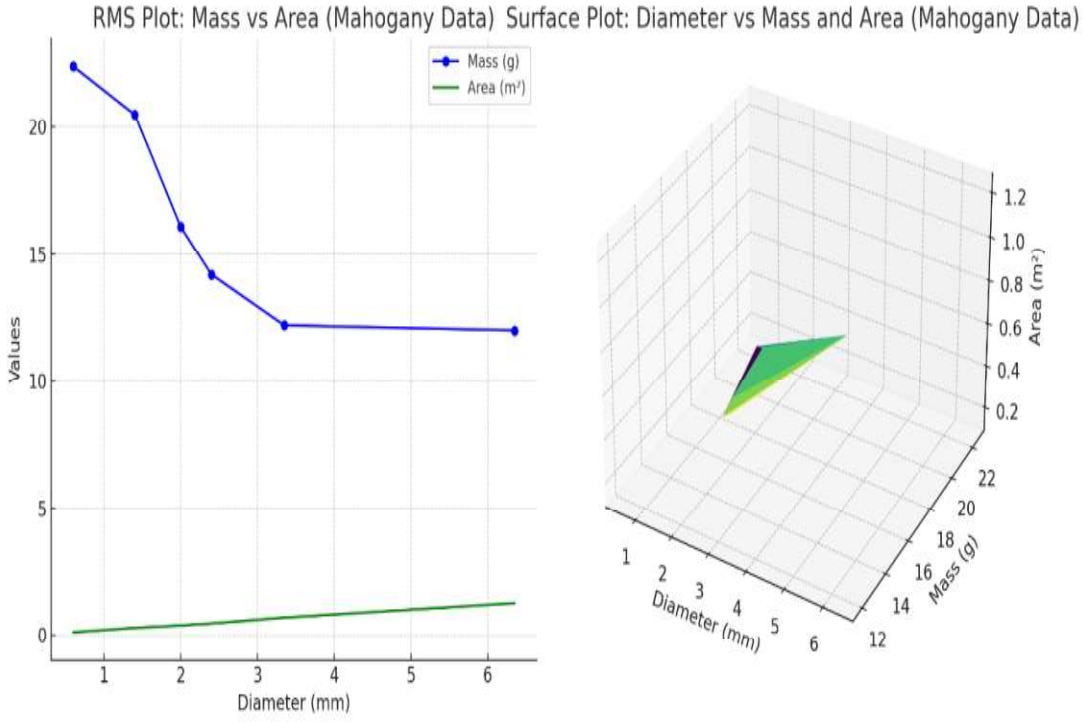

Figure 6: **(a)** RMS plot: Mass Vs area (Mahogany data) **(b)** Surface plot: Diameter Vs Mass and Area (Mahogany Data)

In the RMS Plot on the left, the x-axis represents the diameter of the samples in millimeters, while the y-axis represents the values of mass in grams and volume in cubic meters. The blue curve with circular markers represents the variation of mass with respect to diameter, and the red curve represents the variation of volume. The blue mass curve exhibits a gradual but consistent decline as diameter increases from approximately 1 mm to 6 mm. This downward trend indicates that the mass of the Iroko samples decreases progressively with increasing

diameter, suggesting that as the samples become larger in diameter, their mass per unit volume diminishes. This could point to a lower density in larger samples, possibly due to changes in internal structure or reduced compactness. On the other hand, the red curve representing volume shows a slow but steady upward progression. As the diameter increases, the volume expands slightly, which aligns with the geometric expectation that larger diameters occupy greater spatial volume.

Figure 6 illustrates the relationship between diameter, mass, and area of Iroko briquettes. The RMS plot shows that mass (blue curve) decreases with increasing diameter, indicating a negative correlation, while area (green curve) increases gradually with diameter. The accompanying 3D surface plot further highlights this interaction, showing a declining mass trend alongside a moderate increase in area as diameter increases, thereby clarifying how the three variables vary together.

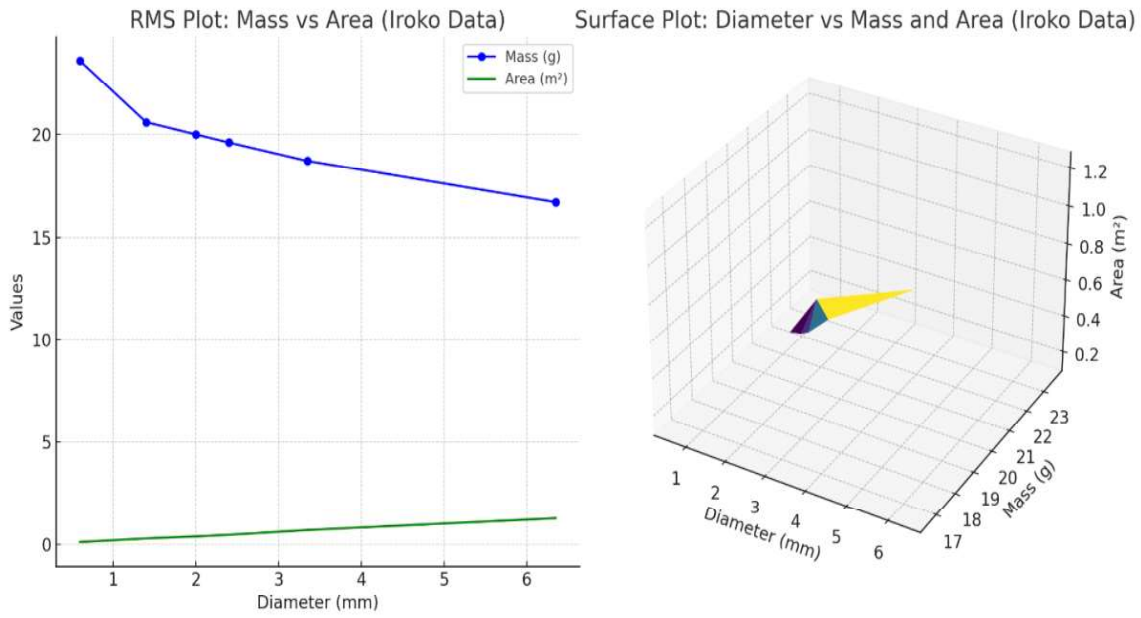

Figure 7: (a) RMS Plot: Mass Vs Area (Iroko data) **(b)** Surface plot: Diameter Vs Mass and Area (Iroko Data)

The figure combines an RMS plot and a surface plot to show the relationship between diameter, mass, and area of Iroko briquettes. In the RMS plot, mass (blue line) decreases sharply with increasing diameter, while area (green line) rises gradually, indicating a strong negative correlation for mass and a weaker positive correlation for area. The RMS value of 19.49 reflects variability in the relationship between mass and area across diameters. Overall, the plots highlight how mass is more sensitive to diameter changes than area, providing insight into the compaction behavior of the briquettes.

4. CONCLUSION

The optimization of process parameters identified the best result based on the highest desirability value of 0.4393. This optimum corresponds to a 0.85 mm diameter Iroko briquette, yielding a density of 0.8390 kg/m³, compaction pressure of 1.467 N/m², moisture content of 31.39%, pore content of 49.29%, ash content of 21.29%, crushing strength of 1153.2 N/m², soot content of 10.49%, boiling rate of 6.95 °C/min, and calorific value of 28.593 kJ/kg. In comparison, a 1.67 mm Mahogany briquette produced lower density (0.4168 kg/m³), lower compaction pressure (0.8771 N/m²), higher pore content (64.59%), and slightly lower calorific value (27.934 kJ/kg). The graph shows strong agreement between predicted and experimental values, validating the model at a 95% confidence level.

5. ACKNOWLEDGEMENT

The author sincerely thanks God Almighty for His guidance throughout this study. Profound gratitude is extended to Engr. Prof. John Wasiu (Dean, Faculty of Engineering) and Engr. Dr. Nihad (Head, Mechanical Engineering) for their mentorship and support. Appreciation is also extended to Engr. Prof. Vincent Balogun, Engr. Oamen, and family for their contributions to my academic journey.

NOMENCLATURE

Greek Symbols

α Thermal expansion coefficient (K^{-1})
β Angle (rad)
γ Specific weight ($N\ m^{-3}$)
δ Deflection of spring (m)
ρ Density ($kg\ m^{-3}$)
$\sigma_{(c)}$ Circumferential stress (Pa)

Subscripts

avg Average value
max Maximum value
min Minimum value
o Initial or reference condition
opt Optimal condition
ref Reference value
w Water
x, y, z Coordinate directions

Superscripts

n Exponent or number of turns
T Transpose
′ First derivative

″ Second derivative

Abbreviations

ANOVA Analysis of Variance
CFD Computational Fluid Dynamics
FEA Finite Element Analysis
FEM Finite Element Method
HVAC Heating, Ventilation, and Air Conditioning
RSM Response Surface Methodology
SI International System of Units
XRD X-Ray Diffraction

REFERENCES

Ajimotokan, H. A., Ibitoye, S. E., Odusote, J. K., Adesoye, O. A., & Omoniyi, P. O. (2019). Physico-mechanical properties of composite briquettes from corncob and rice husk. Journal of Bioresources and Bioproducts, 4(3), 159–165.

Akowuah, J. O., Kemausuor, F., & Mitchual, S. J. (2012). Physico-chemical characteristics and market potential of sawdust charcoal briquette. International Journal of Energy and Environmental Engineering, 3, 20.

Khalid, Y., Tahir, A., Akhtar, N., Khan, I., Tahir, F., Arshad, M., & Raza, A. (2025). From waste to energy: Investigating sawdust combustion as a cleaner alternative to coal. Carbon Neutral Systems, 1, 10.

Motuma, S. (2025). The production and characterization of charcoal briquette from Juniperus procera sawdust as alternative energy source in Sheger City, Ethiopia. Ambo University.

Mtei, A. K., & Mrema, C. B. (2024). Effects of gum arabic as binder on the physico-mechanical properties of briquettes from corn cobs. Mechanical and Thermal Engineering Innovations, 2(1), 23–30.

Okwara, W. M., Nyaanga, D. M., & Kabok, P. (2022). Effect of three feedstocks mix on briquettes' physical and combustion properties. Journal of Engineering in Agriculture and the Environment, 8(2), 45–54.

Oliy, G. B., & Muleta, D. T. (2020). Characterization and determination of briquette fuel prepared from five varieties of corn cob. International Journal of Sustainable and Green Energy, 9(3), 59–64.

Omoniyi, A. O., Adewoye, M. O., & Ogunbayo, O. A. (2025). Characterization of briquettes made from low- and high-density wood sawdust mixed with palm kernel shell. Journal of Renewable Biomass Systems, 9(2), 77–84.

Omoniyi, I. K., Zakka, Y. I., & Owolabi, A. A. (2018). The effect of binder type on the

physico-chemical and calorific compositions of fuel briquette produced from maize cob, sugarcane bagasse and discarded polyethene composite. Tropical Journal of Natural Product Research, 2(9), 418–421.

Owusu, E. K. (2025). Assessment of fuel briquettes from blends of low- and high-density wood sawdust with palm kernel shell residues. International Journal of Renewable, Green, and Sustainable Energy.

PubMed. (2024). Characterization, optimization and emission analysis of manually-made charcoal dust briquettes with starch, paper and algae binders. Renewable Energy Reports, 10, 14–24.

ResearchGate. (2025a). Combustion performance and physicochemical characteristics of sawdust-based bio-charcoal briquettes using molasses adhesive. Renewable Energy and Sustainable Engineering Journal, 7(1), 1–10.

ResearchGate. (2025b). The effect of adhesive ratio on the quality of charcoal briquettes. International Journal of Biomass Energy Science, 6(2), 55–63.

Roman, K., & Grzegorzewska, E. (2024). Biomass briquetting technology for sustainable energy solutions: Innovations in forest biomass utilization. Energies, 17(24), 6392.